3D printed PEEK/HA composites for bone tissue engineering applications: effect of material formulation on mechanical performance and bioactive potential

Faisal Manzoor[1], Atefeh Golbang[1], Swati Jindal[1], Dorian Dixon[2], Alistair McIlhagger[1], Eileen Harkin-Jones[1], Daniel Crawford[3], Elena Mancuso[2*]*

[1] Department of Mechanical Engineering, School of Engineering, Ulster University, Shore Road, BT37 0QB, Newtownabbey, United Kingdom

[2] Nanotechnology and Integrated Bio-Engineering Centre (NIBEC), Ulster University, Shore Road, BT37 0QB, Newtownabbey, United Kingdom

[3] Axial 3D, Alexander House, 17a Ormeau Ave, BT2 8HD, Belfast, United Kingdom

* Corresponding authors emails: manzoor-f@ulster.ac.uk (Faisal Manzoor), e.mancuso@ulster.ac.uk (Elena Mancuso)

Highlights

- PEEK and PEEK-based composite filaments were prepared by extrusion method.
- Fused deposition modelling revealed a promising manufacturing technology for the successful production of 3D printed PEEK/HA composites.
- No significant differences, in terms of mechanical behavior, were detected following the addition of the inorganic phases to the polymeric PEEK matrix.
- 3D printed PEEK/HA composites showed better *in vitro* bioactive performance in comparison to pure PEEK samples.

Abstract

Polyetheretherketone (PEEK) is a biocompatible polymer widely used for biomedical applications. Because it is biologically inert, bioactive phases, such as nano-hydroxyapatite (HA), have been added to PEEK in order to improve its bioactivity. 3D printing (3DP)

technologies are being increasingly used today to manufacture patient specific devices and implants. However, given the challenging processing conditions for PEEK, mainly deriving from its high melting temperature (> 300 °C), the manufacture of PEEK-based composites via 3DP is still in its early stages. In this study, PEEK-based filaments containing 10 wt.% of pure nano-HA, strontium (Sr)- doped nano-HA and Zinc (Zn)-doped nano-HA were produced via hot-melt extrusion and subsequently 3D printed *via* fused deposition modelling (FDM), following an initial optimization process. The raw materials, extruded filaments and 3D printed samples were characterized in terms of physicochemical, thermal and morphological analysis. Moreover, the mechanical performance of 3D printed specimens was assessed *via* tensile tensing. Although an increase in the melting point and a reduction in crystallization temperature was observed with the addition of HA and doped HA to pure PEEK, there was no noticeable increase in the degree of crystallinity. Regarding the mechanical behavior, no significant differences were detected following the addition of the inorganic phases to the polymeric matrix, although a small reduction in the ultimate tensile strength (~ 14%) and Young's modulus (~ 5%) in PEEK/HA was observed in comparison to pure PEEK. Moreover, *in vitro* bioactivity of 3D printed samples was evaluated via a simulated body fluid immersion test for up to 28 days; the formation of apatite was observed on the surfaces of sample surfaces containing HA, SrHA and ZnHA. These results indicate the potential to produce bioactive, 3DP PEEK composites for challenging applications such as in craniofacial bone repair.

Keywords: PEEK, PEEK/HA composites, additive manufacturing, extrusion-based 3D printing.

1 Introduction

Polyaryletherketones (PAEKs) are a group of high-temperature thermoplastic polymers. The most popular among these polymers is PEEK which is commonly used as a biomedical material in bone implant applications.(Kurtz and Devine, 2007) PEEK is a semi-crystalline thermoplastic polymer with excellent mechanical properties, low density, high-temperature durability, chemical stability, and radiolucency. PEEK has an elastic modulus (3-4 GPa) close to that of human trabecular bone (1 GPa), which is much lower than Titanium (Ti) (102-110 GPa) (Han et al., 2019; Najeeb et al., 2016; Sandler et al., 2002). This helps to reduce the stress-shielding effect between an implant and bone, which is the major cause of Ti implant failure (de Araújo Nobre et al., 2019a; de Araújo Nobre et al., 2019b; Lee et al., 2012; Najeeb et al., 2016). In addition, PEEK is a radiolucent material and produces no artifacts during X-ray radiography, computed tomography (CT) or magnetic resonance imaging (MRI), in post-operative assessment which is another drawback associated with metallic implants.(Ma and Tang, 2014) Moreover, PEEK offers excellent stability in sterilization processes (steam or gamma irradiation) due to the aromatic backbone in its structure (Jarman-Smith, 2008; Kumar et al., 2018). However, PEEK is bioinert and offers poor adhesion to the surrounding host tissues (Zhao et al., 2012).

Synthetic hydroxyapatite (HA) (chemical formula $Ca_{10}(PO_4)_6(OH)_2$) is a bioceramic that chemically resembles the naturally occurring mineral phase of bone (Roeder et al., 2008) and has therefore been used clinically as a bone substitute material due to its excellent biocompatibility and bioactivity (Silva et al., 2005). Moreover, the use of trace elements in the HA lattice, such as Strontium (Sr) and Zinc (Zn) has been found to enhance specific biological responses. Particularly, it has been demonstrated that Sr ions stimulate bone formation by increasing osteoid formation, promote osteoblast cell proliferation and enhance Alkaline Phosphatase (ALP) activity (Pierantozzi et al., 2020) while Zn has the additional ability to

stimulate antimicrobial properties (Evis and Webster, 2011; Graziani et al., 2018; Thian et al., 2013). HA alone is a brittle material and hence is not suitable for repairing large defects (Akao et al., 1981). However, HA is used with polymers either as a coating or reinforcing phase to enhance their bioactive properties. The development of composite structures based on PEEK and bioactive ceramics, including HA and its doped formulations has been broadly investigated in the literature (Bakar et al., 2003a; Bakar et al., 2003b; Converse et al., 2007; Garcia-Gonzalez et al., 2017; Wang et al., 2010; Wang et al., 2011). Yu *et. al*. prepared PEEK/HA composites with 10 vol%, 20 vol%, 30 vol% & 40 vol% HA by compaction and pressure-less sintering. They reported that the rate of apatite formation in simulated body fluid (SBF) was directly related to HA percentage (Yu et al., 2005). Ma *et. al.* evaluated the bioactivity of PEEK/HA composites prepared by injection molding with varying HA amounts (0, 10, 20, 30 and 40 wt.%) and evaluated in-vitro bioactivity through SBF immersion test for up to 28 days. They reported that the cell attachment, proliferation and spreading, and ALP activity improved more than pure PEEK due to the presence of HA. They also investigated the effect of HA percentage on the mechanical properties and reported that the tensile strength decreased as the HA content increased (Ma and Guo, 2019a). A similar outcome, (decreasing tensile strength with increasing percentage of HA) was also reported by Bakar *et. al.* (Abu Bakar et al., 2003). Moreover, PEEK/SrHA samples (SrHA: 15 to 30 vol%) prepared by the compression molding technique, demonstrated a decrease in bending strength compared to pure PEEK (25% and 29% decrease with 25 vol% and 30 vol% SrHA, respectively), and proved good bioactivity in SBF after 14 days in immersion, cell proliferation and alkaline phosphatase activity (ALP) in *in-vitro* studies (Wong et al., 2009b).

PEEK and its composite implants have been previously fabricated using conventional manufacturing techniques, such as milling, injection molding and compression molding (Abu Bakar et al., 2003; Conrad and Roeder, 2020; Deng et al., 2015; Rego et al., 2015). However,

these conventional techniques have limitations as they lack customization, precision, complexity and control of internal geometry (Ventola, 2014). Moreover, they are time consuming and expensive (Stansbury and Idacavage, 2016). Only recently, additive manufacturing (AM) has started to be used as a forming process for fabricating PEEK components. AM, which is also referred as three-dimensional (3D) printing or rapid prototyping, is a manufacturing technique in which an object is formed after depositing material layer-by-layer (Ventola, 2014). AM is a revolutionary technology that provides an excellent degree of design freedom with high dimensional accuracy and it can produce complex shapes beyond the limit of conventional technologies (Rinaldi et al., 2018){Saeed, 2021 #385}. The technique is particularly suited to the manufacture of biomedical implants as the parts can be customised to the needs of each patient, thus overcoming the constraints of conventional production approaches. Among the different types of AM, PEEK and its composites have been mainly processed by selective laser sintering (SLS) (Berretta et al., 2018; Schmidt et al., 2007) and Fused Deposition Modeling (FDM) (Berretta et al., 2017; Rinaldi et al., 2018; Wang et al., 2019). For example, PEEK/HA (Hao et al., 2006; Peng et al., 2017; Tan et al., 2003; Tan et al., 2005) and PEEK with carbon fibers (Stepashkin et al., 2018) were processed by SLS and FDM, respectively. Recently, Rodzen *et. al.* reported successful 3D printing of PEEK/HA composite with up to 30 wt.% HA directly from filaments. The tensile strength of the 3D printed PEEH/HA composites was in the range of 79.5–94.2 MPa (Rodzeń, 2021). Oladapo *et. al*. prepared porous PEEK/HA scaffolds via FDM and reported that the tensile strength decreases as the percentage of HA increases, but there was no significant change in strength with additions of up to 10 wt.% HA. In addition, the scaffolds demonstrated cell attachment and proliferation in MG-63 cell line (Oladapo et al., 2020). Vaezi *et. al.* prepared PEEK/HA composite scaffolds by combining the extrusion free forming and compression molding

techniques and optimized the compression molding parameters (pressure, temperature and dwelling time) with HA microstructure to produce a biocomposite (Vaezi and Yang, 2015).

There is currently little published work on PEEK/HA and PEEK/doped HA composites produced via FDM technology. FDM is one of the most widely used and cost-effective additive manufacturing techniques for fabricating prototypes and functional parts from common engineering and high-performance plastics. However, it is often challenging to produce an ideal performance PEEK 3D printed object by FDM due to its elevated melting point, high viscosity, semi-crystalline nature, and high shrinkage after cooling (Golbang et al., 2020) and the printing of PEEK/HA composites via FDM may be potentially more difficult than pure PEEK due to the presence of HA fillers which will alter the viscoelastic and thermomechanical properties of the matrix.

The aim of this study was to design and develop novel PEEK/doped-HA nanocomposites *via* FDM for use in biomedical applications. Overall, three different sets of samples were produced, namely PEEK/HA, PEEK/SrHA and PEEK/ZnHA (10 wt.% bioceramic). Pure PEEK was used as a control in all the experiments performed. Starting from the raw materials in their powder form, filaments were produced via hot melt extrusion and afterwards processed into 3D printed composite structures using FDM. Subsequently, the filaments and the printed samples were characterized in terms of morphological (SEM), thermal (DSC/TGA), mechanical and *in vitro* bioactive behavior through SBF immersion.

2 Materials and methods

2.1 Materials for HA and doped HA synthesis and filament extrusion

PEEK powder was supplied by Evonik (VESTAKEEP® 2000 UFP, GmbH Germany). Calcium Hydroxide [$Ca(OH)_2$, with ACS reagent ≥95%], orthophosphoric acid (H_3PO_4, with 85% purity), Ammonium Hydroxide (NH_4OH), Calcium Nitrate [$Ca(NO_3)_2.4H_2O$], Strontium

Nitrate [$Sr(NO_3)_2$] and Zinc Nitrate Hexahydrate [$Zn(NO_3)_2.6H_2O$] were purchased from Sigma Aldrich. Deionised water (DI) was provided by Fisher Scientific UK.

2.1.1 Synthesis of hydroxyapatite and doped hydroxyapatite

HA and doped HA were prepared via the wet precipitation method, as reported elsewhere (Lowry et al., 2018). In brief, for production of pure hydroxyapatite (HA), $Ca(OH)_2$ suspension was initially stirred in DI water at 400 RPM for 1 h at 60 °C. An aqueous solution of H_3PO_4 was added dropwise to calcium hydroxide solution at the rate of 3.5 ml/min. pH of the mixture was monitored and adjusted to ≥9 with NH_4OH solution. The mixture was further stirred for 2 h and left to age for 24 h. Then the settled precipitates were washed 3 times with DI water. Precipitates were ground to a fine powder with pestle and mortar after being dried at 80 °C in a drying oven for 24 h (Lowry et al., 2018). In order to produce Sr (Sr, 5% by wt.) and Zn (Zn, 5% by wt.) doped HA, their respective salts $Sr(NO_3)_2$ and $Zn(NO_3)_2.6H_2O$, were mixed in an aqueous solution of calcium nitrate and then the same procedure used for the production of pure HA was applied. 5 wt.% Sr and Zn were selected because it was reported that a minimum 5% Sr in HA showed good osteointegration in biological studies (Ni et al., 2011; Tao et al., 2016). Additionally, Chen *et. al.* performed mechanical tests with varying amount of Sr in HA and reported the best mechanical properties with 5 wt.% Sr in HA (Chen and Fu, 2001).

The dried powders were labelled as HA, SrHA, ZnHA and sintered in a furnace (Nabertherm) with a heating ramp of 10 °C/min followed by isothermal condition at 900 °C for 4 h. The samples were then cooled in the furnace. Finally, the heat-treated HA powders were sieved using a mesh size 180 µm.

2.2 Preparation of filaments

The raw PEEK and hydroxyapatite (HA, SrHA and ZnHA) powders were manually blended at concentrations of 10 wt.% and dried overnight in a drying oven at 80 °C before

further usage. A desktop commercial extruder (3devo Composer 450) was used to produce 1.75 ± 0.05 mm diameter filaments of PEEK and PEEK/HA, PEEK/SrHA, PEEK/ZnHA composites.

2.3 3D printing of samples

Fused Deposition Modelling (FDM) of samples was carried out using a commercial SpiderBot 4.0 HT 3D printer equipped with printing-bed and internal chamber heating. Computer-Aided Design (CAD) files of tensile samples (ISO 527-2 Type 5A) in STL format were sliced using the CURA Slicer. Then, Cura Slicer software transformed the CAD files into GCodes which contain the information to control the movement of the printing head in the XYZ-plane, layer height, printing speed and temperatures. The material was deposited layer by layer and after each layer the print head moved in the Z-direction with a distance equal to the layer thickness and the layers fused to form the final 3D object. The starting point for determining the optimum printing parameters were selected from the reported literature. It was observed that a lower bed and chamber temperatures resulted in poor adhesion of the first layer and warpage in the final printed samples, respectively. A summary of the final selected FDM processing parameters is given in Table 1.

Table 1. Printing parameters used to print PEEK and its composites.

Parameter	**Extruded PEEK**	**PEEK/HA**	**PEEK/SrHA**	**PEEK/ZnHA**
Temperature				
Chamber Temperature (°C)	75			
Bed Temperature (°C)	150			
Nozzle Temperature (°C)	370	400	400	400
Nozzle Diameter (mm)	0.5			
Layer				

Layer Height (mm)	0.2
Initial Layer Height (mm)	0.4
Infill	
Infill Density (%)	100
Infill pattern	Concentric
Orientation (°)	0
Speed	
Print Speed (mm/s)	30
Infill Speed (mm/s)	30
Initial Layer Speed (mm/s)	15

The main difference between the optimum printing conditions for pure PEEK filaments and PEEK/HA nanocomposites is the enhanced nozzle temperature from 370 °C to 400 °C, respectively. The need for a higher nozzle temperature to achieve better print quality in the case of PEEK/HA nanocomposites could be due to the altered heat transfer/thermal conduction of the composite, an increase in PEEK viscosity and/or an increase in the melting point of PEEK due to the addition of 10 wt.% HA and doped HA. (please refer to section 3.5.)

2.4 Physicochemical characterisation

Particle size and morphology of the materials in the powder form along with surface morphology and distribution of HA particles in the 3D printed samples were observed through SEM (FESEM HITACHI, Japan) at 15kV under high vacuum with working distance ~5.5 mm. All samples were gold sputter coated before analysis. The elemental composition, purity of the raw materials and distribution of doping elements in HA were analysed using an EDX machine (Oxford Instruments Ltd.) with Aztec software at 20kV.

The samples were analysed using FTIR (Thermoscientific iD5) in Attenuated Total Reflection (ATR) mode with resolution 8 cm^{-1} and range from 4000 cm^{-1} to 550 cm^{-1}.

The thermal properties (melting temperature, crystallization temperature and crystallization degree) and thermal degradation of PEEK, PEEK/HA, PEEK/SrHA and PEEK/ZnHA filaments were analysed by Differential Scanning Calorimetry (DSC, TA Instruments Q100) and Thermogravimetric Analysis (TGA, TA Instruments Q600), respectively. In both cases, samples were heated at a rate of 10 °C/minute. TGA curves were obtained by heating samples from 25 °C to 700 °C in a nitrogen atmosphere. DSC curves were obtained by heating samples from 25 °C to 450 °C with a heat-cool-heat cycle at a rate of 10 °C/minute. The degree of crystallinity by weight (X_{CW} %) was evaluated by using the formula:

$$X_{CW}\ (\%) = \quad H_m / (W_f \times H_c)$$

Where H_m is the melting enthalpy obtained from DSC scan, W_f is the weight fraction of PEEK in composite and H_c is the melting enthalpy of fully crystallized PEEK (130J/g) (Sikder et al., 2020a).

2.5 Mechanical characterisation

Tensile testing was carried out using an Instron testing machine (Instron 3344) and following the ISO standard: ISO 527-2 Type 5A.(ISO, 1996) Five specimens (75 mm x 4 mm x 2 mm) were tested for each sample with a crosshead speed of 2.0 mm/minute at 20 °C and using a 2 kN load cell.

2.6 *In vitro* bioactivity assessment

Simulated body fluid (SBF) was prepared according to Kokubo's protocol in which the solution has nearly the same ion concentration as human blood plasma (Na^+ 142.0 mM, K^+ 5.0 mM, Mg^{2+} 1.5mM, Ca^{2+} 2.5mM, Cl^- 147.8mM, $HCO3^-$ 4.2mM, $HPO4^{2-}$ 1.0mM, $SO4^{2-}$ 0.5mM, pH 7.40 at 36.5 °C) (Kokubo and Takadama, 2006). All 3D printed samples (disk

shaped, 10 mm Dia) (PEEK, PEEK/HA, PEEK/SrHA, PEEK/ZnHA) (n=3) were immersed in 15 mL of SBF and stored at 37 °C. The solution was replenished once a week. After 7, 14 and 28 days, the samples were washed with DI water and dried at 37 °C for 24 h. Then, the surfaces of the samples were characterized *via* SEM and EDX. The samples were first sputter gold coated and then observed under SEM (FESEM HITACHI, Japan) at 10.0 kV. The apatite layer was analysed by EDX (Oxford Instruments Ltd.) at 20 kV attached with SEM.

3 Results and discussion

3.1 Raw materials for filament preparation

3.1.1 SEM and EDX

Particle size and morphology of HA, SrHA and ZnHA powders were analysed by SEM and shown in Figure 1 (A to H). As observed in Figure 1 (A-low magnification image and B-high magnification image), the PEEK powder particles are spherical with an average particle size of ~10 μm. The particle size of HA, SrHA and ZnHA powders were originally in the nanometer range. It is possible that, due to high sintering temperature (900 °C) they partly fused together and formed agglomerates (Figure 1C to 1H). Similar particle fusion after sintering of HA has been reported elsewhere (Ai et al., 2011). From Figure 1(C&D), it can be seen that the HA particles are spherical with a particle size in the range of 50 nm to 100 nm. The morphology of SrHA and ZnHA is shown in Figure 1(E-low magnification image & F-high magnification image) and Figure 1(G-low magnification image & H-high magnification image) respectively. The particles were originally spherical and in nanometer range however, due to high temperature sintering (900 °C), the nanoparticles fused together to form agglomerates. This phenomenon has also been reported elsewhere (Muralithran and Ramesh, 2000; Scalera et al., 2020). The fusion of particles can be seen more prominently in the SrHA and ZnHA samples. This may be due to the presence of the doping elements (Sr and Zn). These

powders were ground and sieved through a 180 µm sieve to avoid any nozzle blockage during printing.

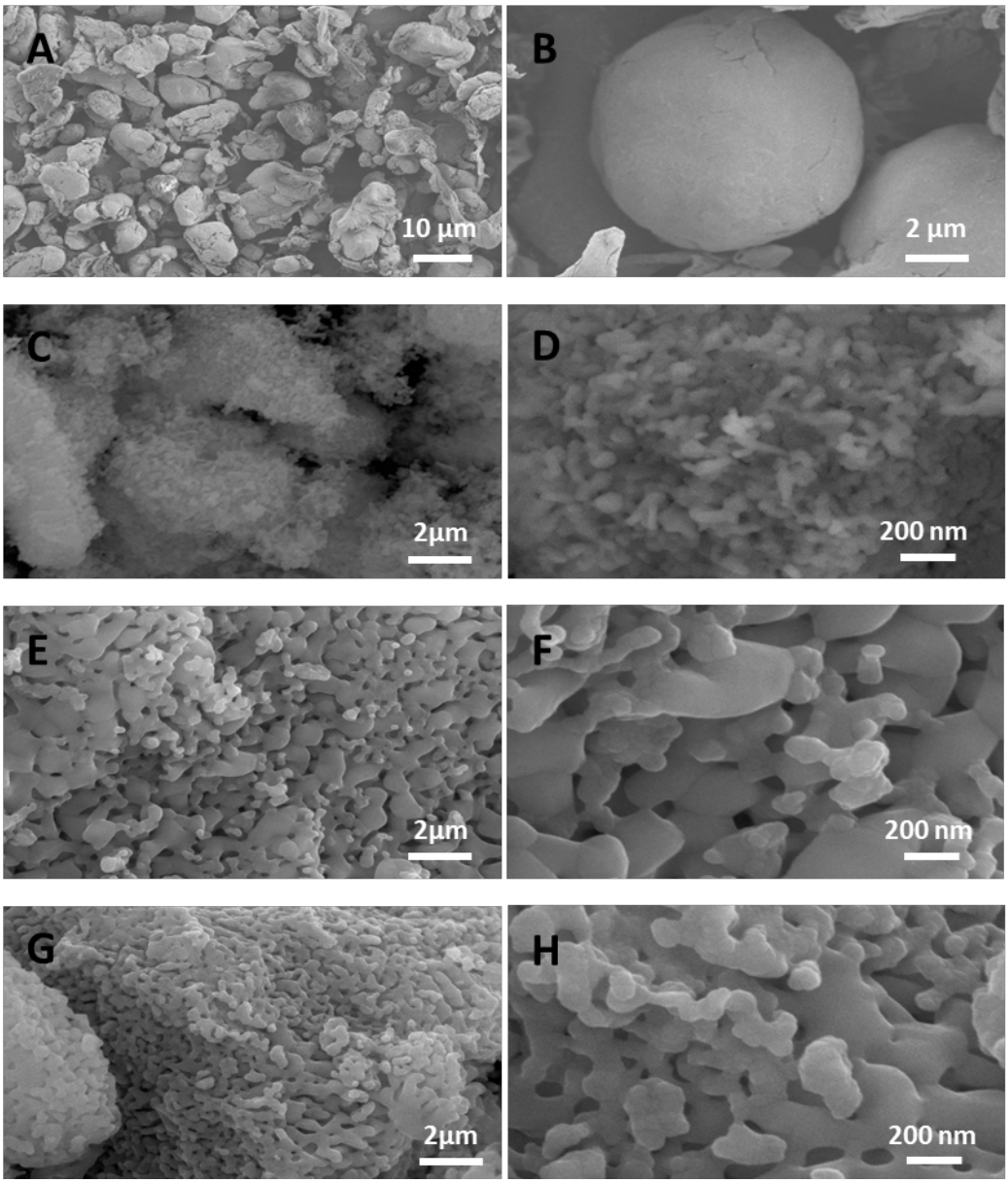

Figure 1 SEM micrographs of: raw PEEK powder (A&B), nano-HA (C&D), Sr doped nano-HA (E&F) and Zn doped nano-HA (G&H) synthesized by wet precipitation method and sintered at 900 °C.

Elemental EDX maps of HA, SrHA and ZnHA are shown in Figure 2. For pure HA, the elemental map of calcium (Ca), phosphorous (P) and oxygen (O) are shown. There were

no major elemental impurities detected, and these elements present homogenously in the HA. Similar results were observed in SrHA and ZnHA with a uniform distribution of Sr and Zn seen in the samples.

	Image	Ca	P	O	Sr	Zn
HA	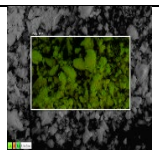	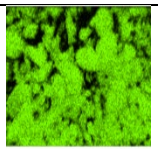	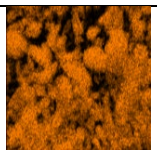	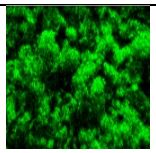	X	X
SrHA	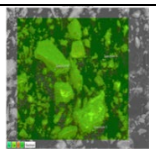	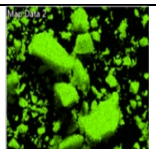	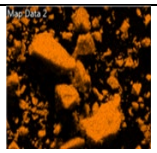	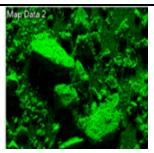	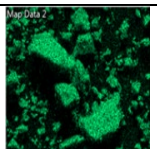	X
ZnHA	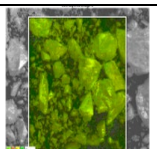	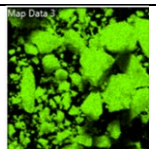	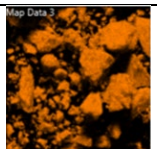	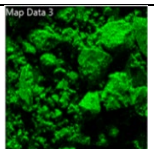	X	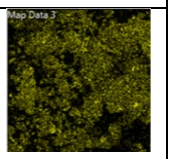

Figure 2. Elemental mapping of HA, SrHA and ZnHA synthesized by wet precipitation method, showing the elemental mapping by EDX analysis.

In Figure 3, elemental analysis of HA, SrHA and ZnHA by EDX is reported. The spectra show the detected elements with their characteristic peaks and confirms that there is not any major impurity.

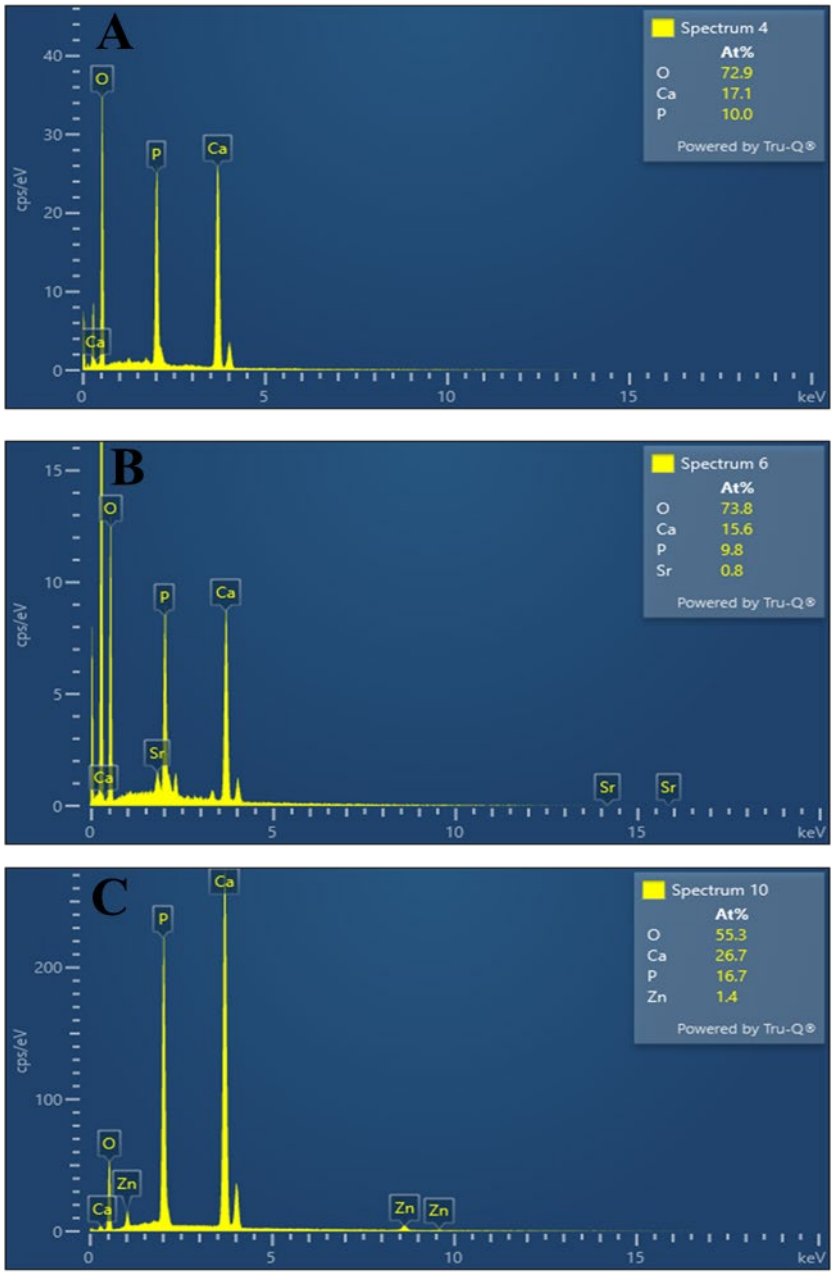

Figure 3 EDX spectra of A) hydroxyapatite, B) strontium doped hydroxyapatite, C) zinc doped hydroxyapatite, synthesized by wet precipitation method and sintered at 900 °C.

3.1.2 FTIR

FTIR spectra of synthesized HA and doped HA powders are shown in Figure 4. The typical stretching vibration of the P-O bond can be seen at 1200 cm^{-1} and 900 cm^{-1}. The fundamental modes of PO_4 tetrahedron can be observed at 1025-1085 cm^{-1} (v_3), with a small

shoulder peak at 960 cm^{-1} (v_1), 562 cm^{-1}, and 604 cm^{-1} (v_4) (El Boujaady et al., 2016). The stretching and bending mode of O-H appear at 630 cm^{-1} and 3550 cm^{-1}, respectively (Siddiqi et al., 2016). However, due to the presence of doping elements (Sr, Zn), a slight shift in peaks can be observed (Norhidayu et al., 2008; Pantasri et al., 2017) in Figure 4. A summary of the peak allocations is presented in Table 2 for understanding.

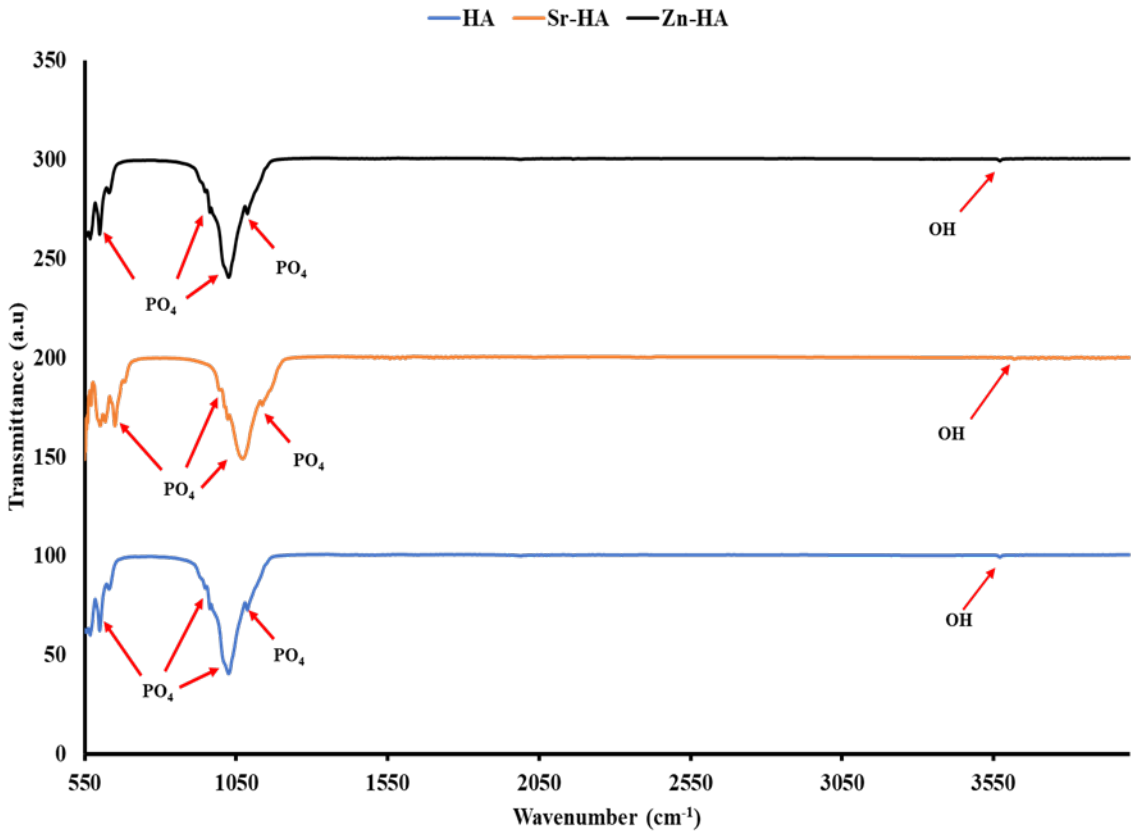

Figure 4. FTIR spectra of A) HA, B) SrHA and C) ZnHA synthesized by wet precipitation method and sintered at 900 °C

Table 2. Summary of peak positioning of hydroxyapatite and doped-hydroxyapatite functional groups.

Material	**$[PO_4]v_4$** **cm^{-1}**	**$[PO_4]v_3$** **cm^{-1}**	**OH** **cm^{-1}**
HA	562, 604	960, 1025, 1092	630, 3550
SrHA	570, 610	980, 1080, 1130	610, 3590
ZnHA	572, 610	975, 1080, 1130	610, 3590

3.2 Filament preparation and characterization

The filaments of PEEK and its composites (PEEK/HA, PEEK/SrHA, PEEK/ZnHA) were prepared for 3D printing by using a desktop extruder. There were four heating zones in the machine from hopper to nozzle (H_4 to H_1). Due to the low density of the raw materials, the powder was fed continuously by pressing manually into the hopper. The screw compounded and pushed the materials forward at a fixed speed. Nip rollers were used to pull the molten material out of the nozzle and cooling fans solidified the melt as it exited the nozzle. The diameter and the quality of the filaments depend on a number of factors: extrusion temperature, extruder screw speed, nip rollers speed, cooling fan speed and feeding rate. The beaded and non-uniform diameter filaments prepared during the optimization process are shown in Figure 5. The machine has a filament diameter sensor. The filaments prepared with measured diameter 1.75 ± 0.05. The optimized parameters were set as follows: for PEEK, temperature increased gradually from hopper to nozzle as H_4=355 °C, H_3=365 °C, H_2=370 °C, H_1=380 °C while for PEEK composites (PEEK/HA, PEEK/SrHA, PEEK/ZnHA) the temperatures were set from hopper to nozzle as H_4=360 °C, H_3=370 °C, H_2=380 °C, H_1=400 °C, the extruder screw speed was set for all filaments at 5.5 RPM, cooling fan with 100% efficiency and nip rollers were set

manually at 650 RPM. The extruded filament was wound onto an empty spool. The filament-spools were dried overnight in a drying oven at 80 °C prior to use for printing and characterization. The filament extrusion parameters for PEEK and its composites are summarized in Table 3.

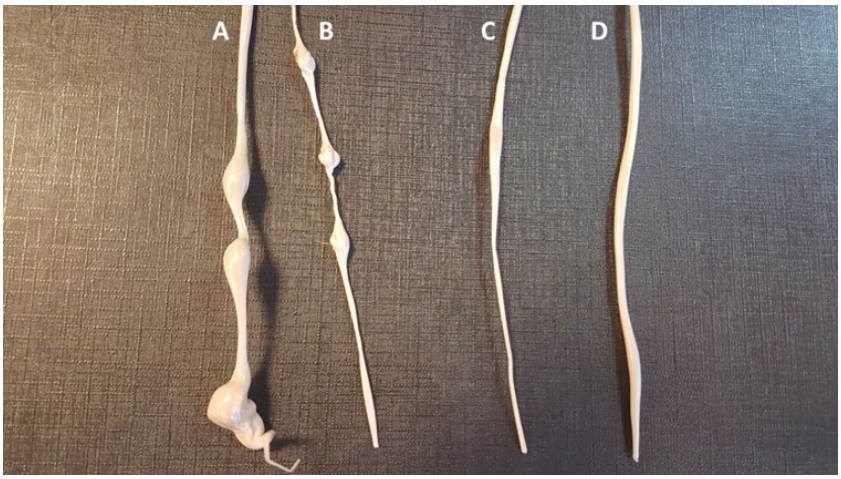

Figure 5. PEEK filaments with beads and non-uniform diameter in the extrusion optimization process produced at different H_1 temperatures A) 360 °C, B) 365 °C, C) 370 °C, D) 380 °C

Table 3. Extrusion parameters to produce filaments of PEEK and its composites.

	PEEK	**PEEK/HA**	**PEEK/SrHA**	**PEEK/ZnHA**
Temperatures				
H_1 (°C)	380	400	400	400
H_2 (°C)	370	380	380	380
H_3 (°C)	360	370	370	370
H_4 (°C)	355	360	360	360
Speed				
Extruder screw speed (RPM)	5.5	5.5	5.5	5.5

Nip rollers speed (RPM)	650	650	650	650
Cooling fan speed (%)	100	100	100	100

3.3 3D printed samples

3.3.1 SEM

The morphology of the printed samples was observed *via* SEM and presented in Figure 6 with low and high magnifications. The distribution of HA and doped-HA in printed samples is shown in Figure 6 (C to H). The presence of ceramic particles and their distribution on the polymer surface were confirmed through SEM. Based on Figure 6, there appears to be larger agglomerates present in the samples containing SrHA and ZnHA particles.

During filament extrusion, some of the ceramic particles were encapsulated in PEEK matrix and some remained at the surface (Rego et al., 2015). Generally, the surface of pure PEEK is hydrophobic and is not suitable for attaching biomolecules and proteins. The presence of HA on the surface of the filament increases its hydrophilicity (Lee et al., 2013; Ma and Guo, 2019a) by acting as bioactive sites for apatite formation, cell attachment and soft tissue adhesion to the surface (Zhao et al., 2016a).

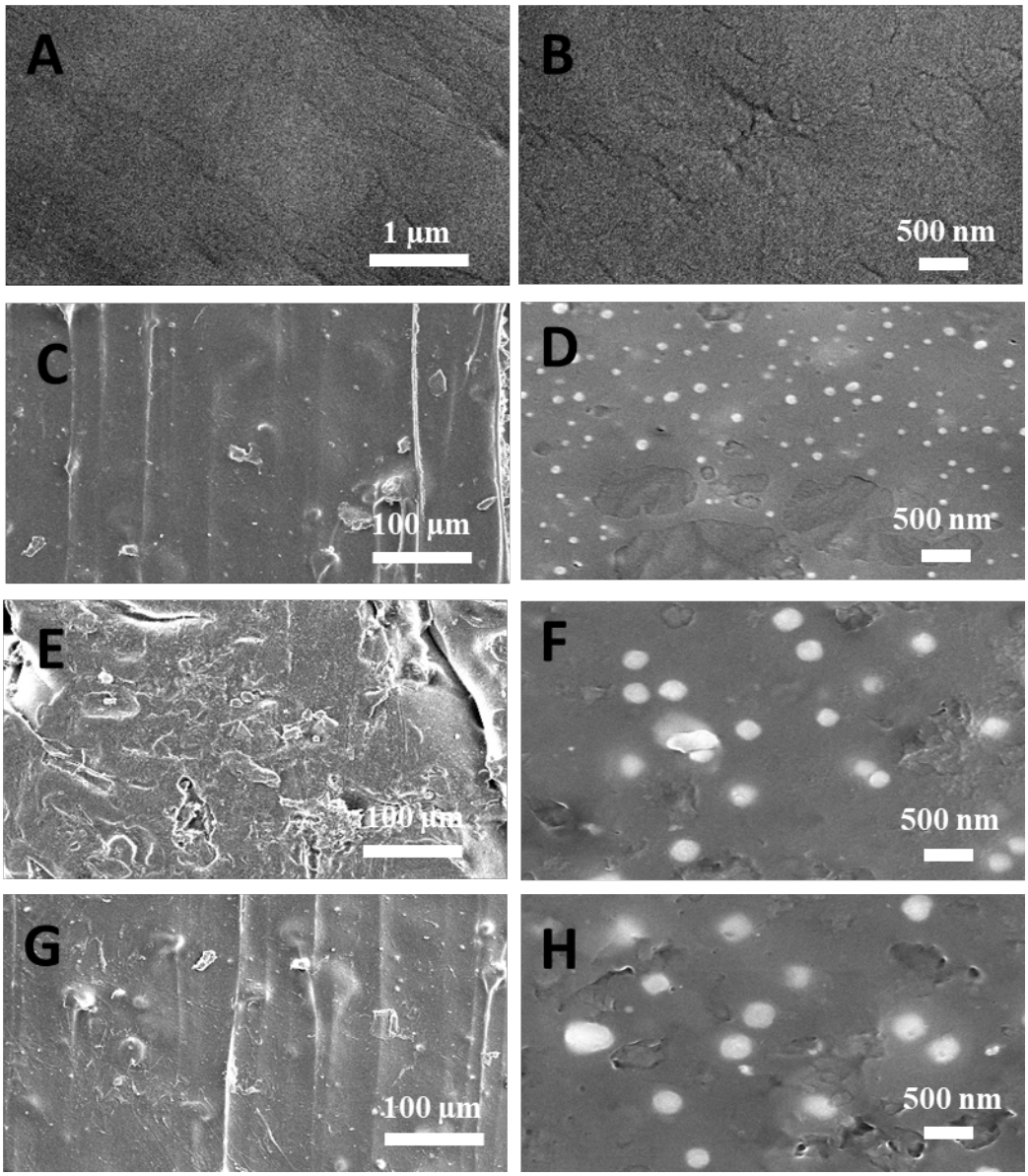

Figure 6. SEM micrographs of FDM 3D printed samples prepared from: in-house extruded PEEK from raw powder (A&B), distribution of nHA particles (C&D), distribution of SrHA particles (E&F), distribution of ZnHA particles at PEEK surface (G&H).

3.3.2 TGA/DSC

Figure 7 shows the TGA curves of PEEK, PEEK/HA, PEEK/SrHA and PEEK/ZnHA filaments. From Figure 7, it is evident that the weight of all samples was constant up to ~600 °C. Degradation began after ~600 °C and samples were completely degraded at ~700 °C. This confirms that there is no degradation during the filament production and 3D-printing since the

processing temperature is well below the degradation temperature of these material. The presence of HA and doped HA in PEEK increases its thermal stability. This is more noticeable in the case of ZnHA. The amount of ceramic in the polymer matrix can be calculated from TGA data (Tan et al., 2005). In the PEEK filament curve, the polymer burnt off without leaving behind any impurity. However, the weight remaining (~10%) at the end of PEEK/HA, PEEK/SrHA and PEEK/ZnHA curves, is due to the presence of the ceramic component of the composite material as 10 wt.% ceramic was added into the PEEK. This also supports the point which was claimed in section 3.3.1 i.e., the uniform distribution of ceramic phase in polymer matrix.

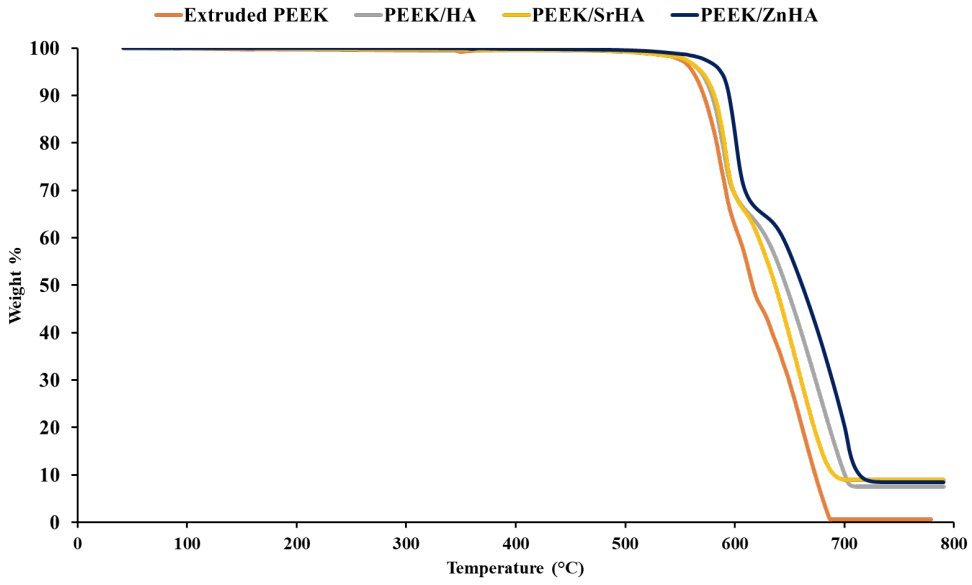

Figure 7. TGA curves for raw PEEK powder, extruded PEEK, PEEK/HA, PEEK/SrHA and PEEK/ZnHA filaments

In Figure 8A, the melting temperatures (T_m) of PEEK, PEEK/HA, PEEK/SrHA and PEEK/ZnHA filaments are shown and it can be seen that the melting points increased when ceramic was added into PEEK. This can be ascribed to the restriction of polymer chain mobility in the presence of HA particles. A similar behavior (increase in melting point with the presence of ceramic) was previously observed in PEEK/ZnO (Hao et al., 2018) and PEEK/carbon nano

tubes (Alam et al., 2020; Díez-Pascual et al., 2010) composites. Hence, PEEK composites possess higher melting points than PEEK leading to a requirement for higher extrusion and printing temperatures. This was also noted during the optimization of filament extrusion mentioned in section 3.2, for selecting the appropriate printing conditions for PEEK and its composites. Figure 8B shows the crystallization temperatures (T_c) of PEEK, PEEK/HA, PEEK/SrHA and PEEK/ZnHA filaments. The crystallization temperature decreased in the presence of HA and doped HA. This may be due to the ceramic particles hindering the nucleation process in PEEK which in turn delayed the crystallization process. The PEEK filament (Figure 8B) exhibits a major crystallization peak (~287 °C) and a small shoulder at a slightly lower temperature (~260 °C) (Anderson et al., 2018). The appearance of a small shoulder at around 260 °C (lower crystallization point) indicates secondary crystallization and the growth of crystals which arise due to the formation of thinner lamella while the higher (or major) crystallization transition (T_c~287 °C) represents primary crystallization due to the formation of the main crystalline lamella (Tan et al., 1999; Verma et al., 1996). The melting point generally is dependent on crystallization temperature and the degree of crystallization which lies some 5 to 70 °C above T_c (Verma et al., 1996).

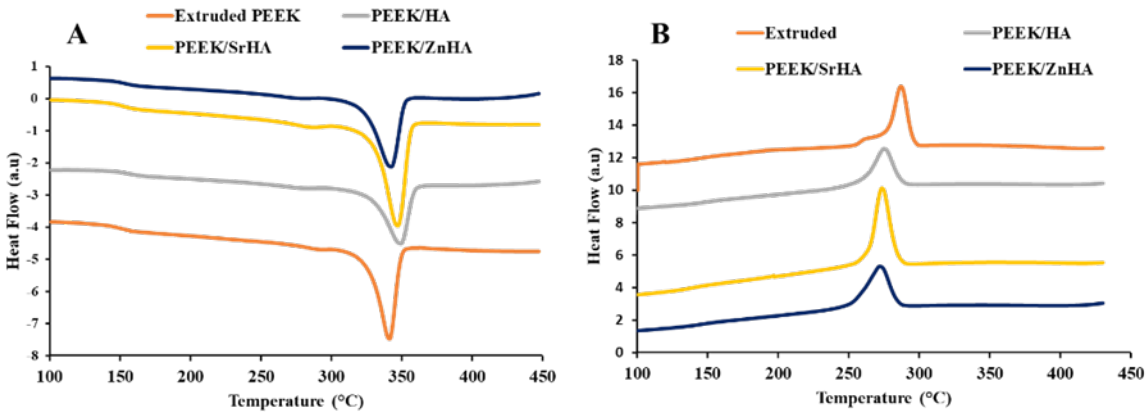

Figure 8. DSC curves showing A) melting temperature (T_m), B) recrystallization temperature (T_c) of PEEK, PEEK/HA, PEEK/SrHA filament and PEEK/ZnHA filaments

The thermal properties of PEEK, PEEK/HA, PEEK/SrHA and PEEK/ZnHA filaments have been summarized below in Table 4. As demonstrated in table 4, there is no significant change in the crystallization percentage of PEEKwith the addition of HA and SrHA.

Table 4. Thermal properties of PEEK, PEEK/HA, PEEK/SrHA and PEEK/ZnHA filaments.

Filament Sample	**T_m (°C)**	**T_c (°C)**	**T_d (°C)**	**H_m (J/g)**	**X_c %**
PEEK	343.1	288.8	593.4	38.5	29.6
PEEK/HA	352.6	277.5	605.2	35.5	30.3
PEEK/SrHA	351.2	275.4	602.7	37.0	31.6
PEEK/ZnHA	348.5	274.2	610.4	34.7	29.6

3.3.3 Tensile testing

Table 5 shows the tensile strength, Young's modulus and % elongation at break of the 3D printed samples comprised of pure PEEK and PEEK with HA and doped HA. The stress-strain curves for these samples are shown in Figure 10.

The purpose of using 10% by wt. HA was to achieve good bioactivity and acceptable mechanical properties (without significant loss of mechanical strength). Although the Young's modulus of bulk HA is very high i.e. approximately 130 GPa (Meyers et al., 2008), it has been previously reported that adding 10 wt.% HA into PEEK slightly changes (from ~90 MPa to 80 MPa) its mechanical properties and the samples possess good biocompatibility (Oladapo et al., 2020). Below the percolation threshold, the factors affecting the mechanical properties of a polymer composite are the size of filler material (Ji et al., 2002) and % crystallinity (Humbert et al., 2011). According to Table 5, the Young's modulus of 3D-printed PEEK is increased from about 789 MPa to 801 MPA with 10 wt.% HA. There is no significant change in PEEK's modulus with addition of 10 wt.% Sr-HA. However, a small reduction in Young's modulus is

noted in the case of PEEK/ZnHA compared with pure PEEK which may be ascribed to a higher degree of agglomeration in this sample.

Based on the presented data in table 5, the tensile strength of pure PEEK is reduced with incorporation of 10 wt.% HA, from 67.90 ± 2.98 MPa to 58.38 ± 4.49 MPa. The tensile strength decreased slightly more when Sr and Zn doped HA were incorporated. This may be due to the larger agglomerate size of Sr and Zn doped HA nano-powders as compared to pure HA, particularly in the latter, as discussed in section 3.1. The elongation decreases with the addition of HA and doped-HA.

The reduction in tensile strength may be due to the bioceramic nature of the particles which act as stress concentrators in the PEEK matrix (due to their poor interfacial adhesion with the PEEK polymer matrix) (Golbang et al., 2020; Jeyachandran et al., 2020). In a study, Ma *et. al.* prepared PEEK/HA composite using an in-situ polymerization process and reported that the percentage decrease in tensile strength was less due to the strong interfacial bonding between the HA and PEEK (Ma et al., 2012), as compared to samples mixed physically (Ma and Guo, 2019a). The tensile strength of the PEEK, PEEK/HA and PEEK/SrHA samples are higher than the lower range of cortical bone (50 MPa) (Hench, 1993). However, the tensile strength of PEEK/ZnHA is slightly lower, which may be due to the formation of large agglomerates (as described in section 3.1.1) during sintering.

Generally, the tensile strength of samples produced by 3D printing are lower than parts produced by injection molding (Jeyachandran et al., 2020). This can be due to imperfect bonding between layers and the presence of voids in 3D printed parts which can reduce their mechanical properties (Petersmann et al., 2020).

Figure 9. Representative image of tensile test samples prepared by FDM

Table 5. Tensile strength of 3D printed PEEK and its composite samples.

Sample	**Tensile Strength (MPa) ± SD**	**Young's modulus (MPa) ± SD**	**Elongation (%) ± SD**
PEEK	67.9 ± 2.9	788.7 ± 52.2	12.8 ± 1.3
PEEK/HA	58.4 ± 4.5	801.2 ± 72.0	8.8 ± 0.6
PEEK/SrHA	51.5 ± 1.1	785.9 ± 22.7	8.9 ± 0.7
PEEK/ZnHA	47.9 ± 0.7	749.6 ± 26.7	8.4 ± 0.7

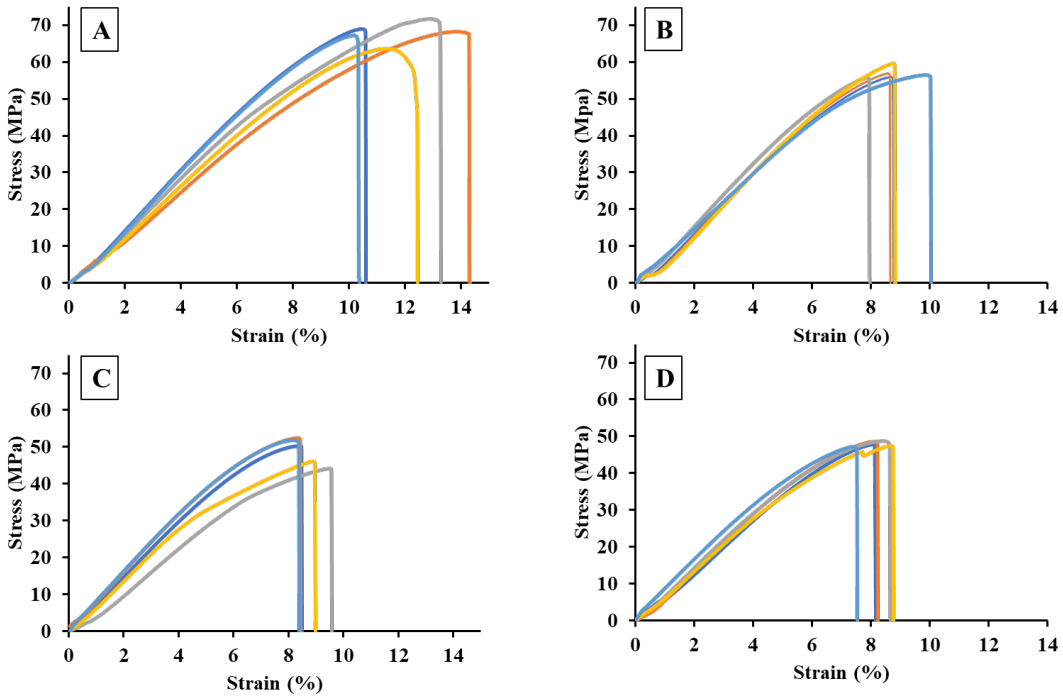

Figure 10. Stress-strain curves of 3D printed samples, A) PEEK, B) PEEK/HA, C) PEEK/SrHA, D) PEEK/ZnHA

3.3.4 In-vitro bioactivity assessment

PEEK has received considerable attention in clinical applications because of its excellent mechanical properties, stability and excellent processability. However, PEEK-based implants are biologically inert. In this perspective, the inclusion of inorganic phases into the polymeric matrix aims to enhance PEEK bioactive characteristics. Bioactivity is a prominent feature that manifest with the formation of a HA-like layer on the surface of a material and thus predicts its bone-bonding ability (Kokubo, 1991). In this study, the bioactivity of 3D printed PEEK-based composites was analysed through the SBF immersion method and then evaluated *via* physico-chemical analysis. It was observed that small islands of precipitates started forming after 7 days of immersion on PEEK/HA, PEEK/SrHA and PEEK/ZnHA samples, as shown in Figure 11. The morphology and EDX results suggested that these small islands of precipitates were apatite particles which started depositing on PEEK composites. The mechanism of apatite

formation on the surface of PEEK composite can be explained by the electrostatic interaction between Ca^{+2} on PEEK/HA surface and anions in SBF solution. Initial nucleation of apatite particles starts due to the capturing of anions (HPO_4^{-2}, OH^{-1}) from the SBF solution by Ca^{+2}. Thus, forming metastable phase of calcium hydrogen phosphate which grows and converts into a stable bone-like apatite phase (Yu et al., 2005). These particles appeared almost equally on PEEK composite samples after 7 days immersion in SBF. The growth of apatite precursors increased after 14 days of immersion, both in terms of size and numbers as shown in Figure 12. After 28 days, PEEK/HA, PEEK/SrHA and PEEK/ZnHA shown a significant amount of apatite precipitates on their surface, as shown in Figure 13; whereas as expected no apatite formation was detected on the surface of pure PEEK. In addition, based on EDX spectra after 28 days in immersion, the small islands on the surfaces of PEEK/HA, PEEK/SrHA and PEEK/ZnHA showed apatite characteristics as demonstrated by the Ca/P ratios (see Table 6). The Ca/P ratios was calculated by dividing the atomic % of Ca and P at different time points, as shown in Table 6. The Ca/P ratios from EDX results suggest that the particles formed after 7 days of immersion are apatite as their ratios are nearly similar to theoretical value i.e., 1.67 (Stanislavov et al., 2018). Similarly, the Ca/P ratios of 14 days and 28 days samples are also nearly equal to the theoretical value of stoichiometric HA (Ca/P=1.67). Hence, this demonstrates that the inclusion of HA, SrHA and ZnHA, within the pure PEEK matrix supports the formation of an apatite-like layer on its surface (Roy and Sailaja, 2015). No considerable differences in terms of apatite formation have been detected among the pure HA and its doped forms as reported by the EDX analysis (see Figure 13 and Table 6), thus suggesting the promise for them all to be used as bioactive phases. Similar phenomenon has also been reported elsewhere in which researchers have demonstrated the improvement of bioactivity in PEEK polymer by incorporating bioactive ceramics. However, the production route adopted to manufacture bioactive PEEK composites has been mainly conventional up to now (Ma and

Guo, 2019b; Rego et al., 2015; Sikder et al., 2020b; Wang et al., 2014; Wong et al., 2009a; Zhao et al., 2016b). Conventional technologies such as injection molding, extrusion etc., have inherent limitations, which include length of the processes, costs and lack of customization while 3D printing allows the fabrication of parts with freedom of design and a range of materials with tailorable properties. Overall, these results suggest the suitability of the manufacturing approach for the fabrication of 3D printed bioactive composites based on PEEK, and the possibility to further extend its use in bone regeneration scenarios.

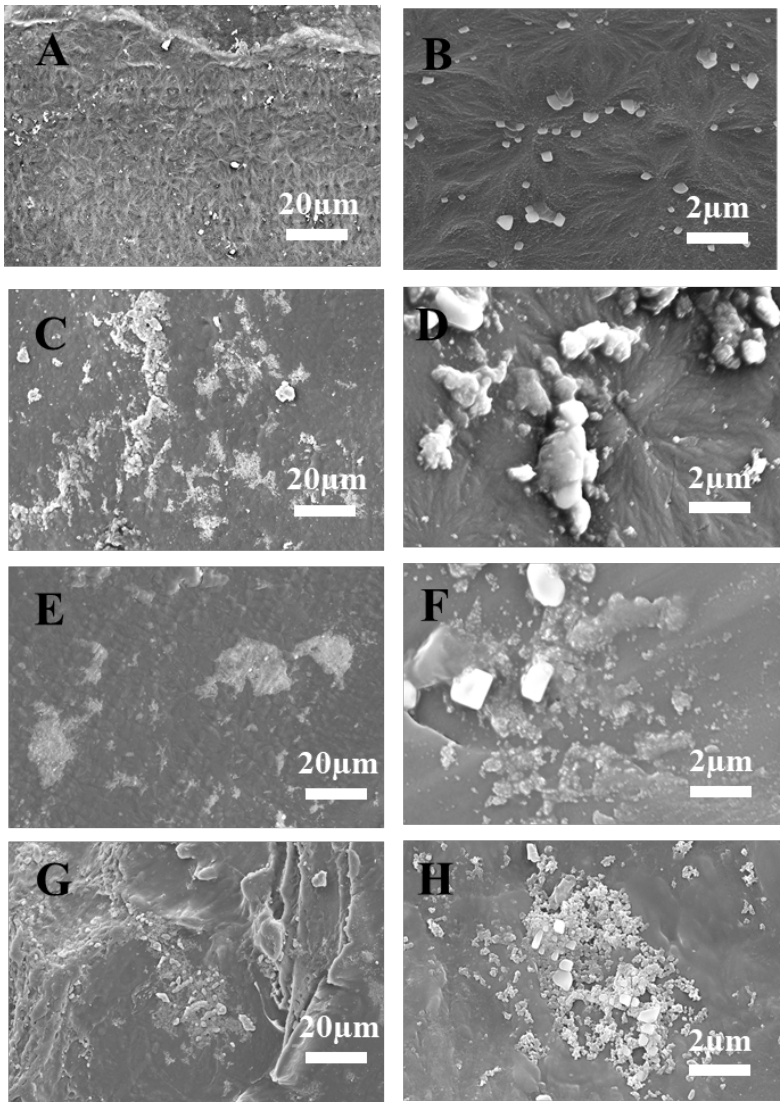

Figure 11 Representative SEM micrographs of samples' surface after immersion in SBF for 7 days: PEEK (A - B), PEEK/HA (C - D), PEEK/SrHA (E - F), PEEK/ZnHA (G - H)

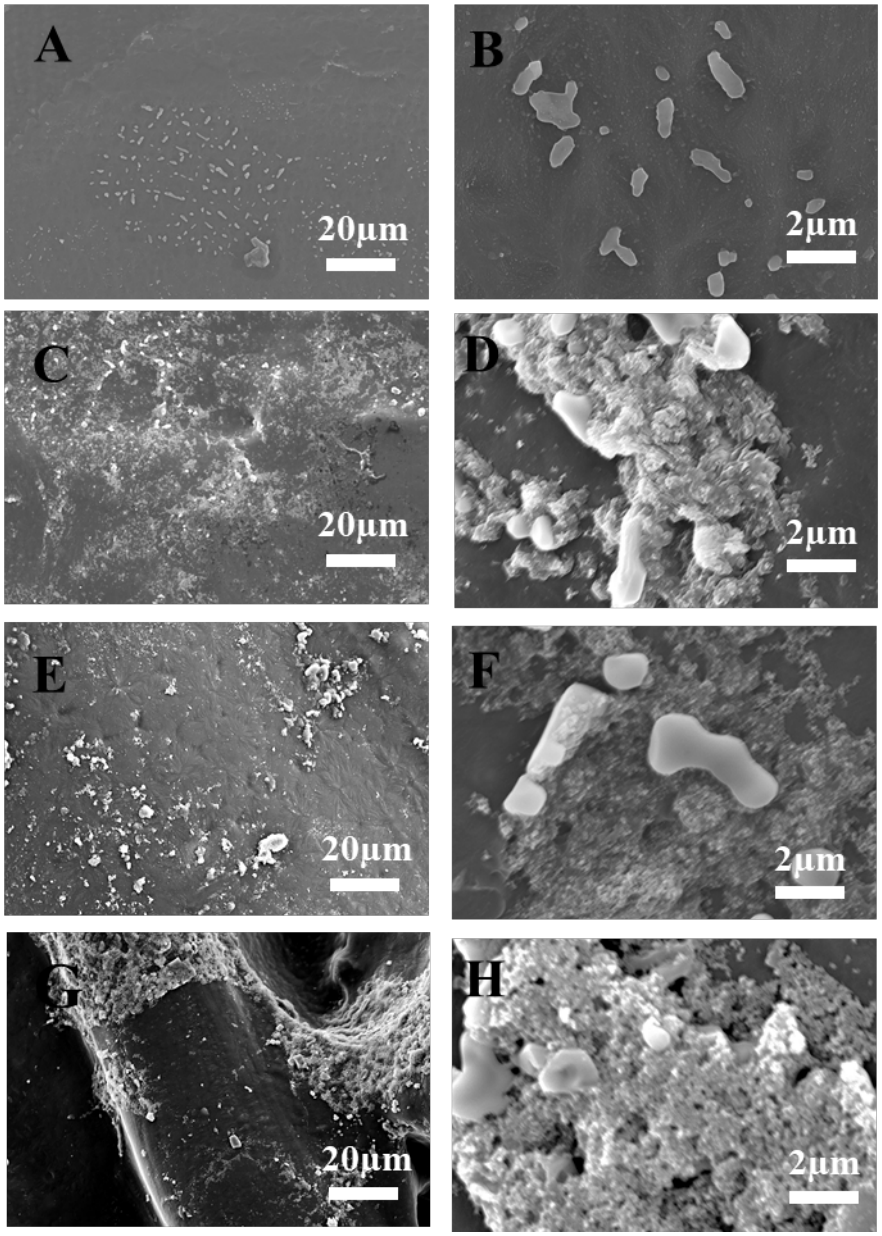

Figure 12 Representative SEM micrographs of samples' surface after immersion in SBF for 14 days: PEEK (A - B), PEEK/HA (C - D), PEEK/SrHA (E - F), PEEK/ZnHA (G - H)

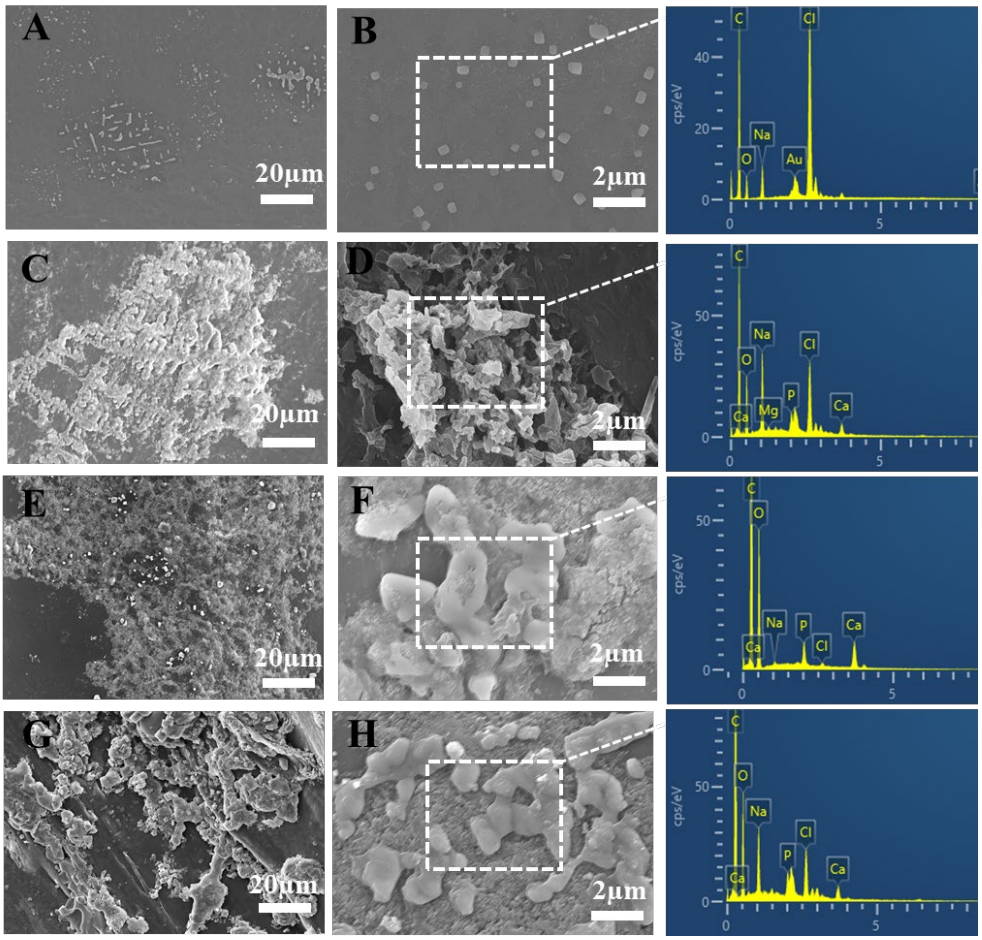

Figure 13 Representative SEM micrographs and EDX of samples surface after immersion in SBF for 28 days: PEEK (A - B), PEEK/HA (C - D), PEEK/SrHA (E - F), PEEK/ZnHA (G - H)

Table 6 Ca/P ratios of the precipitates formed on the surface of samples and measured by EDX analysis

	PEEK	PEEK/HA	PEEK/SrHA	PEEK/ZnHA
Day 7	Ca/P = 0	Ca/P = 1.59	Ca/P = 1.62	Ca/P = 1.60
Day 14	Ca/P = 0	Ca/P = 1.69	Ca/P = 1.71	Ca/P = 1.74
Day 28	Ca/P = 0	Ca/P = 1.73	Ca/P = 1.77	Ca/P = 1.72

4 Conclusion

In this work, PEEK nanocomposites with 10 wt.% HA, SrHA and ZnHA were extruded into filament and then 3D printed via FDM technology, which provides a solution to rapid prototyping of customized and cost-effective bioactive orthopedic/dental implants. In the first step, HA and doped HA were synthesized and characterized by SEM, EDX and FTIR. Then, filaments of PEEK, PEEK/HA, PEEK/SrHA and PEEK/ZnHA with diameter of 1.75 ± 0.05 mm were produced via melt mixing after optimization and thereafter used for 3D printing of samples. The printing conditions were optimized to achieve a good print quality. Thermal analysis showed that the melting points of PEEK composites increased by the addition of HA and doped HA while there was no significant effect on the crystallinity of PEEK. Also, the chemical structure of each sample remained intact after 3D printing via FDM. Based on the tensile testing data, the Young's modulus was not grossly affected by the presence of 10 wt.% HA, SrHA and ZnHA. However, there was a small reduction in the ultimate tensile strength (up to about 15%) and elongation at break with the addition of HA, SrHA and ZnHA to PEEK. SBF studies confirmed the improvement of PEEK *in* vitro bioactivity following the inclusion of HA and its doped forms. Taken together these results suggest the promise of FDM 3D printing in combination with PEEK-based composites for the development of patient-specific bioactive implants and its potential in orthopedic and maxillofacial applications.

Acknowledgement

The North West Centre for Advanced Manufacturing (NW CAM) project is supported by the European Union's INTERREG VA Programme, managed by the Special EU Programmes Body (SEUPB). The views and opinions in this document do not necessarily reflect those of the European Commission or the Special EU Programmes Body (SEUPB).

If you would like further information about NW CAM please contact the lead partner, Catalyst, for details.

CRediT authorship contribution statement

Faisal Manzoor: Conceptualization, Methodology, Investigation, Writing - Original Draft **Atefeh Golbang:** Writing - Review & Editing, Supervision, Project administration **Swati Jindal:** Writing - Review & Editing **Dorian Dixon:** Writing - Review & Editing, Supervision, Project administration **Alistair McIlhagger:** Project administration **Eileen Harkin-Jones:** Funding acquisition, Writing - Review & Editing **Daniel Crawford:** Resources **Elena Mancuso:** Conceptualization, Methodology, Writing - Review & Editing, Supervision, Project administration

Declaration of competing interest

The authors declare that they have no known competing financial interests or personal relationships that could have appeared to influence the work reported in this paper.

References

Abu Bakar, M.S., Cheang, P., Khor, K.A., 1999. Thermal processing of hydroxyapatite reinforced polyetheretherketone composites. Journal of Materials Processing Technology 89-90, 462-466.

Abu Bakar, M.S., Cheng, M.H.W., Tang, S.M., Yu, S.C., Liao, K., Tan, C.T., Khor, K.A., Cheang, P., 2003. Tensile properties, tension–tension fatigue and biological response of polyetheretherketone–hydroxyapatite composites for load-bearing orthopedic implants. Biomaterials 24, 2245-2250.

Ai, J., Rezaei-Tavirani, M., Biazar, E., Heidari, K., Jahandideh, R., 2011. Mechanical properties of chitosan-starch composite filled hydroxyapatite micro-and nanopowders. Journal of Nanomaterials 2011.

Akao, M., Aoki, H., Kato, K., 1981. Mechanical properties of sintered hydroxyapatite for prosthetic applications. Journal of Materials Science 16, 809-812.

Alam, F., Varadarajan, K.M., Koo, J.H., Wardle, B.L., Kumar, S., 2020. Additively manufactured polyetheretherketone (PEEK) with carbon nanostructure reinforcement for biomedical structural applications. Advanced Engineering Materials 22, 2000483.

Anderson, L.J., Yuan, X., Fahs, G.B., Moore, R.B., 2018. Blocky Ionomers via Sulfonation of Poly (ether ether ketone) in the Semicrystalline Gel State. Macromolecules 51, 6226-6237.

Bakar, M.A., Cheang, P., Khor, K., 2003a. Mechanical properties of injection molded hydroxyapatite-polyetheretherketone biocomposites. Composites Science and Technology 63, 421-425.
Bakar, M.A., Cheng, M., Tang, S., Yu, S., Liao, K., Tan, C., Khor, K., Cheang, P., 2003b. Tensile properties, tension–tension fatigue and biological response of polyetheretherketone–hydroxyapatite composites for load-bearing orthopedic implants. Biomaterials 24, 2245-2250.
Berretta, S., Davies, R., Shyng, Y., Wang, Y., Ghita, O., 2017. Fused Deposition Modelling of high temperature polymers: Exploring CNT PEEK composites. Polymer Testing 63, 251-262.
Berretta, S., Evans, K., Ghita, O., 2018. Additive manufacture of PEEK cranial implants: Manufacturing considerations versus accuracy and mechanical performance. Materials & Design 139, 141-152.
Chen, D., Fu, Y., 2001. Evaluation on the mechanical properties of the solid solution of strontium substituted hydroxyapatite. Chin J Stoma Mater Appar 19, 178-183.
Conrad, T.L., Roeder, R.K., 2020. Effects of porogen morphology on the architecture, permeability, and mechanical properties of hydroxyapatite whisker reinforced polyetheretherketone scaffolds. Journal of the Mechanical Behavior of Biomedical Materials 106, 103730.
Converse, G.L., Yue, W., Roeder, R.K., 2007. Processing and tensile properties of hydroxyapatite-whisker-reinforced polyetheretherketone. Biomaterials 28, 927-935.
de Araújo Nobre, M., Ferro, A., Maló, P., 2019a. Adult patient risk stratification using a risk score for periodontitis. J Clin Med 8, 307.
de Araújo Nobre, M., Salvado, F., Nogueira, P., Rocha, E., Ilg, P., Maló, P., 2019b. A Peri-Implant Disease Risk Score for Patients with Dental Implants: Validation and the Influence of the Interval between Maintenance Appointments. J Clin Med 8, 252.
Deng, Y., Liu, X., Xu, A., Wang, L., Luo, Z., Zheng, Y., Deng, F., Wei, J., Tang, Z., Wei, S., 2015. Effect of surface roughness on osteogenesis in vitro and osseointegration in vivo of carbon fiber-reinforced polyetheretherketone–nanohydroxyapatite composite. International journal of nanomedicine 10, 1425.
Díez-Pascual, A.M., Naffakh, M., González-Domínguez, J.M., Ansón, A., Martínez-Rubi, Y., Martinez, M.T., Simard, B., Gómez, M.A., 2010. High performance PEEK/carbon nanotube composites compatibilized with polysulfones-II. Mechanical and electrical properties. Carbon 48, 3500-3511.
El Boujaady, H., Mourabet, M., El Rhilassi, A., Bennani-Ziatni, M., El Hamri, R., Taitai, A., 2016. Adsorption of a textile dye on synthesized calcium deficient hydroxyapatite (CDHAp): kinetic and thermodynamic studies. J. Mater. Environ. Sci 7, 4049-4063.
Evis, Z., Webster, T., 2011. Nanosize hydroxyapatite: doping with various ions. Advances in Applied Ceramics 110, 311-321.
Garcia-Gonzalez, D., Jayamohan, J., Sotiropoulos, S., Yoon, S.-H., Cook, J., Siviour, C., Arias, A., Jérusalem, A., 2017. On the mechanical behaviour of PEEK and HA cranial implants under impact loading. Journal of the mechanical behavior of biomedical materials 69, 342-354.
Golbang, A., Harkin-Jones, E., Wegrzyn, M., Campbell, G., Archer, E., McIlhagger, A., 2020. Production and characterization of PEEK/IF-WS2 nanocomposites for additive manufacturing: Simultaneous improvement in processing characteristics and material properties. Additive Manufacturing 31, 100920.
Graziani, G., Boi, M., Bianchi, M., 2018. A review on ionic substitutions in hydroxyapatite thin films: Towards complete biomimetism. Coatings 8, 269.
Han, X., Yang, D., Yang, C., Spintzyk, S., Scheideler, L., Li, P., Li, D., Geis-Gerstorfer, J., Rupp, F., 2019. Carbon fiber reinforced PEEK composites based on 3D-printing technology for orthopedic and dental applications. J Clin Med 8, 240.

Hao, L., Hu, Y., Zhang, Y., Wei, W., Hou, X., Guo, Y., Hu, X., Jiang, D., 2018. Enhancing the mechanical performance of poly (ether ether ketone)/zinc oxide nanocomposites to provide promising biomaterials for trauma and orthopedic implants. RSC advances 8, 27304-27317.
Hao, L., Savalani, M., Zhang, Y., Tanner, K., Harris, R., 2006. Selective laser sintering of hydroxyapatite reinforced polyethylene composites for bioactive implants and tissue scaffold development. Proceedings of the Institution of Mechanical Engineers, Part H: Journal of Engineering in Medicine 220, 521-531.
Hench, L.L., 1993. An introduction to bioceramics. World scientific.
Humbert, S., Lame, O., Séguéla, R., Vigier, G., 2011. A re-examination of the elastic modulus dependence on crystallinity in semi-crystalline polymers. Polymer 52, 4899-4909.
ISO, B., 1996. 527-2: 1996. Plastics—determination of tensile properties—part 2: test conditions for moulding and extrusion plastics. British Standards Institution, 1-14.
Jarman-Smith, M., 2008. Evolving uses for implantable PEEK and PEEK based compounds. Medical device technology 19, 12-15.
Jeyachandran, P., Bontha, S., Bodhak, S., Balla, V.K., Kundu, B., Doddamani, M., 2020. Mechanical behaviour of additively manufactured bioactive glass/high density polyethylene composites. Journal of the Mechanical Behavior of Biomedical Materials 108, 103830.
Ji, X.L., Jing, J.K., Jiang, W., Jiang, B.Z., 2002. Tensile modulus of polymer nanocomposites. Polymer Engineering & Science 42, 983-993.
Kokubo, T., 1991. Bioactive glass ceramics: properties and applications. Biomaterials 12, 155-163.
Kokubo, T., Takadama, H., 2006. How useful is SBF in predicting in vivo bone bioactivity? Biomaterials 27, 2907-2915.
Kumar, A., Yap, W.T., Foo, S.L., Lee, T.K., 2018. Effects of sterilization cycles on PEEK for medical device application. Bioengineering 5, 18.
Kurtz, S.M., Devine, J.N., 2007. PEEK biomaterials in trauma, orthopedic, and spinal implants. Biomaterials 28, 4845-4869.
Lee, J.H., Jang, H.L., Lee, K.M., Baek, H.-R., Jin, K., Hong, K.S., Noh, J.H., Lee, H.-K., 2013. In vitro and in vivo evaluation of the bioactivity of hydroxyapatite-coated polyetheretherketone biocomposites created by cold spray technology. Acta Biomaterialia 9, 6177-6187.
Lee, W.T., Koak, J.Y., Lim, Y.J., Kim, S.K., Kwon, H.B., Kim, M.J., 2012. Stress shielding and fatigue limits of poly-ether-ether-ketone dental implants. Journal of Biomedical Materials Research Part B: Applied Biomaterials 100, 1044-1052.
Lowry, N., Brolly, M., Han, Y., McKillop, S., Meenan, B.J., Boyd, A.R., 2018. Synthesis and characterisation of nanophase hydroxyapatite co-substituted with strontium and zinc. Ceramics International 44, 7761-7770.
Ma, R., Guo, D., 2019a. Evaluating the bioactivity of a hydroxyapatite-incorporated polyetheretherketone biocomposite. Journal of Orthopaedic Surgery and Research 14, 32.
Ma, R., Guo, D., 2019b. Evaluating the bioactivity of a hydroxyapatite-incorporated polyetheretherketone biocomposite. Journal of orthopaedic surgery and research 14, 1-13.
Ma, R., Tang, T., 2014. Current strategies to improve the bioactivity of PEEK. International journal of molecular sciences 15, 5426-5445.
Ma, R., Weng, L., Bao, X., Ni, Z., Song, S., Cai, W., 2012. Characterization of in situ synthesized hydroxyapatite/polyetheretherketone composite materials. Materials Letters 71, 117-119.
Meyers, M.A., Chen, P.-Y., Lin, A.Y.-M., Seki, Y., 2008. Biological materials: structure and mechanical properties. Progress in Materials Science 53, 1-206.
Mijovic, J., Gsell, T.C., 1990. Calorimetric study of polyetheretherketone (PEEK) and its carbon fiber composite. SAMPE quarterly 21, 42-46.

Muralithran, G., Ramesh, S., 2000. The effects of sintering temperature on the properties of hydroxyapatite. Ceramics International 26, 221-230.
Najeeb, S., Zafar, M.S., Khurshid, Z., Siddiqui, F., 2016. Applications of polyetheretherketone (PEEK) in oral implantology and prosthodontics. Journal of prosthodontic research 60, 12-19.
Ni, G.-X., Yao, Z.-P., Huang, G.-T., Liu, W.-G., Lu, W.W., 2011. The effect of strontium incorporation in hydroxyapatite on osteoblasts in vitro. Journal of Materials Science: Materials in Medicine 22, 961-967.
Norhidayu, D., Sopyan, I., Ramesh, S., 2008. Development of zinc doped hydroxyapatite for bone implant applications, ICCBT 2008 Conference, pp. 257-270.
Oladapo, B.I., Zahedi, S.A., Ismail, S.O., Omigbodun, F.T., Bowoto, O.K., Olawumi, M.A., Muhammad, M.A., 2020. 3D printing of PEEK–cHAp scaffold for medical bone implant. Bio-Design and Manufacturing, 1-16.
Pantasri, T., Seet, S., Suwanna, P., 2017. Preparation of strontium-and/or zinc-doped hydroxyapatite nanoparticles and their polycaprolactone composite fibrous scaffolds, Journal of Physics: Conference Series. IOP Publishing, p. 012029.
Peng, S., Feng, P., Wu, P., Huang, W., Yang, Y., Guo, W., Gao, C., Shuai, C., 2017. Graphene oxide as an interface phase between polyetheretherketone and hydroxyapatite for tissue engineering scaffolds. Scientific reports 7, 46604.
Petersmann, S., Spoerk, M., Van De Steene, W., Üçal, M., Wiener, J., Pinter, G., Arbeiter, F., 2020. Mechanical properties of polymeric implant materials produced by extrusion-based additive manufacturing. journal of the mechanical behavior of biomedical materials 104, 103611.
Pierantozzi, D., Scalzone, A., Jindal, S., Stīpniece, L., Šalma-Ancāne, K., Dalgarno, K., Gentile, P., Mancuso, E., 2020. 3D printed Sr-containing composite scaffolds: Effect of structural design and material formulation towards new strategies for bone tissue engineering. Composites Science and Technology 191, 108069.
Rego, B.T., Neto, W.A.R., de Paula, A.C.C., Góes, A.M., Bretas, R.E.S., 2015. Mechanical properties and stem cell adhesion of injection-molded poly (ether ether ketone) and hydroxyapatite nanocomposites. Journal of Applied Polymer Science 132.
Rinaldi, M., Ghidini, T., Cecchini, F., Brandao, A., Nanni, F., 2018. Additive layer manufacturing of poly (ether ether ketone) via FDM. Composites Part B: Engineering 145, 162-172.
Roeder, R.K., Converse, G.L., Kane, R.J., Yue, W., 2008. Hydroxyapatite-reinforced polymer biocomposites for synthetic bone substitutes. Jom 60, 38-45.
Roy, P., Sailaja, R., 2015. Mechanical, thermal and bio-compatibility studies of PAEK-hydroxyapatite nanocomposites. Journal of the mechanical behavior of biomedical materials 49, 1-11.
Sandler, J., Werner, P., Shaffer, M.S., Demchuk, V., Altstädt, V., Windle, A.H., 2002. Carbon-nanofibre-reinforced poly (ether ether ketone) composites. Composites Part A: Applied Science and Manufacturing 33, 1033-1039.
Scalera, F., Palazzo, B., Barca, A., Gervaso, F., 2020. Sintering of magnesium-strontium doped hydroxyapatite nanocrystals: Towards the production of 3D biomimetic bone scaffolds. Journal of Biomedical Materials Research Part A 108, 633-644.
Schmidt, M., Pohle, D., Rechtenwald, T., 2007. Selective Laser Sintering of PEEK. CIRP Annals 56, 205-208.
Siddiqi, S.A., Manzoor, F., Jamal, A., Tariq, M., Ahmad, R., Kamran, M., Chaudhry, A., Rehman, I.U., 2016. Mesenchymal stem cell (MSC) viability on PVA and PCL polymer coated hydroxyapatite scaffolds derived from cuttlefish. RSC Advances 6, 32897-32904.

Sikder, P., Ferreira, J.A., Fakhrabadi, E.A., Kantorski, K.Z., Liberatore, M.W., Bottino, M.C., Bhaduri, S.B., 2020a. Bioactive amorphous magnesium phosphate-polyetheretherketone composite filaments for 3D printing. Dental Materials.
Sikder, P., Ferreira, J.A., Fakhrabadi, E.A., Kantorski, K.Z., Liberatore, M.W., Bottino, M.C., Bhaduri, S.B., 2020b. Bioactive amorphous magnesium phosphate-polyetheretherketone composite filaments for 3D printing. Dental Materials 36, 865-883.
Silva, R., Camilli, J., Bertran, C., Moreira, N., 2005. The use of hydroxyapatite and autogenous cancellous bone grafts to repair bone defects in rats. International journal of oral and maxillofacial surgery 34, 178-184.
Stanislavov, A.S., Sukhodub, L.F., Sukhodub, L.B., Kuznetsov, V.N., Bychkov, K.L., Kravchenko, M.I., 2018. Structural features of hydroxyapatite and carbonated apatite formed under the influence of ultrasound and microwave radiation and their effect on the bioactivity of the nanomaterials. Ultrasonics Sonochemistry 42, 84-96.
Stansbury, J.W., Idacavage, M.J., 2016. 3D printing with polymers: Challenges among expanding options and opportunities. Dental Materials 32, 54-64.
Stepashkin, A., Chukov, D., Senatov, F., Salimon, A., Korsunsky, A., Kaloshkin, S., 2018. 3D-printed PEEK-carbon fiber (CF) composites: Structure and thermal properties. Composites Science and Technology 164, 319-326.
Tan, K., Chua, C., Leong, K., Cheah, C., Cheang, P., Bakar, M.A., Cha, S., 2003. Scaffold development using selective laser sintering of polyetheretherketone–hydroxyapatite biocomposite blends. Biomaterials 24, 3115-3123.
Tan, K., Chua, C., Leong, K., Naing, M., Cheah, C., 2005. Fabrication and characterization of three-dimensional poly (ether-ether-ketone)/-hydroxyapatite biocomposite scaffolds using laser sintering. Proceedings of the Institution of Mechanical Engineers, Part H: Journal of Engineering in Medicine 219, 183-194.
Tan, S., Su, A., Luo, J., Zhou, E., 1999. Crystallization kinetics of poly (ether ether ketone)(PEEK) from its metastable melt. Polymer 40, 1223-1231.
Tao, Z.-S., Bai, B.-L., He, X.-W., Liu, W., Li, H., Zhou, Q., Sun, T., Huang, Z.-L., Tu, K.-k., Lv, Y.-X., Cui, W., Yang, L., 2016. A comparative study of strontium-substituted hydroxyapatite coating on implant's osseointegration for osteopenic rats. Medical & Biological Engineering & Computing 54, 1959-1968.
Thian, E., Konishi, T., Kawanobe, Y., Lim, P., Choong, C., Ho, B., Aizawa, M., 2013. Zinc-substituted hydroxyapatite: a biomaterial with enhanced bioactivity and antibacterial properties. Journal of Materials Science: Materials in Medicine 24, 437-445.
Vaezi, M., Yang, S., 2015. A novel bioactive PEEK/HA composite with controlled 3D interconnected HA network. International journal of Bioprinting 1.
Ventola, C.L., 2014. Medical applications for 3D printing: current and projected uses. Pharmacy and Therapeutics 39, 704.
Verma, R.K., Velikov, V., Kander, R.G., Marand, H., Chu, B., Hsiao, B.S., 1996. SAXS studies of lamellar level morphological changes during crystallization and melting in PEEK. Polymer 37, 5357-5365.
Wang, L., He, S., Wu, X., Liang, S., Mu, Z., Wei, J., Deng, F., Deng, Y., Wei, S., 2014. Polyetheretherketone/nano-fluorohydroxyapatite composite with antimicrobial activity and osseointegration properties. Biomaterials 35, 6758-6775.
Wang, L., Weng, L., Song, S., Sun, Q., 2010. Mechanical properties and microstructure of polyetheretherketone–hydroxyapatite nanocomposite materials. Materials Letters 64, 2201-2204.
Wang, L., Weng, L., Song, S., Zhang, Z., Tian, S., Ma, R., 2011. Characterization of polyetheretherketone–hydroxyapatite nanocomposite materials. Materials Science and Engineering: A 528, 3689-3696.

Wang, P., Zou, B., Xiao, H., Ding, S., Huang, C., 2019. Effects of printing parameters of fused deposition modeling on mechanical properties, surface quality, and microstructure of PEEK. Journal of Materials Processing Technology 271, 62-74.
Wong, K., Wong, C., Liu, W., Pan, H., Fong, M., Lam, W., Cheung, W., Tang, W., Chiu, K., Luk, K., 2009a. Mechanical properties and in vitro response of strontium-containing hydroxyapatite/polyetheretherketone composites. Biomaterials 30, 3810-3817.
Wong, K.L., Wong, C.T., Liu, W.C., Pan, H.B., Fong, M.K., Lam, W.M., Cheung, W.L., Tang, W.M., Chiu, K.Y., Luk, K.D.K., Lu, W.W., 2009b. Mechanical properties and in vitro response of strontium-containing hydroxyapatite/polyetheretherketone composites. Biomaterials 30, 3810-3817.
Yu, S., Hariram, K.P., Kumar, R., Cheang, P., Aik, K.K., 2005. In vitro apatite formation and its growth kinetics on hydroxyapatite/polyetheretherketone biocomposites. Biomaterials 26, 2343-2352.
Zhao, M., An, M., Wang, Q., Liu, X., Lai, W., Zhao, X., Wei, S., Ji, J., 2012. Quantitative proteomic analysis of human osteoblast-like MG-63 cells in response to bioinert implant material titanium and polyetheretherketone. Journal of proteomics 75, 3560-3573.
Zhao, M., Li, H., Liu, X., Wei, J., Ji, J., Yang, S., Hu, Z., Wei, S., 2016a. Response of human osteoblast to n-HA/PEEK—quantitative proteomic study of bio-effects of nano-hydroxyapatite composite. Scientific reports 6, 22832.
Zhao, M., Li, H., Liu, X., Wei, J., Ji, J., Yang, S., Hu, Z., Wei, S., 2016b. Response of human osteoblast to n-HA/PEEK—quantitative proteomic study of bio-effects of nano-hydroxyapatite composite. Scientific reports 6, 1-13.